Giant Spin Gap and Magnon Localization in the Disordered Heisenberg Antiferromagnet $Sr_2Ir_{1-x}Ru_xO_4$ Supplementary Information

Yue Cao,[1,*] Xuerong Liu,[2,†] Wenhu Xu,[1,‡] Weiguo Yin,[1] D. Meyers,[1] Jungho Kim,[3] Diego Casa,[3] Mary Upton,[3] Thomas Gog,[3] Tom Berlijn,[4] Gonzalo Alvarez,[4] Shujuan Yuan,[5] Jasminka Terzic,[5] J. M. Tranquada,[1] John P. Hill,[6] Gang Cao,[5,7] Robert M. Konik,[1] and M. P. M. Dean[1,§]

[1] *Condensed Matter Physics and Material Science Department, Brookhaven National Laboratory, Upton, NY 11973*
[2] *Institute of Physics, Chinese Academy of Sciences, Beijing 100190, China*
[3] *Advanced Photon Source, Argonne National Laboratory, Lemont, IL 60439, U.S.A.*
[4] *Computer Science and Mathematics Division and Center for Nanophase Materials Sciences, Oak Ridge National Laboratory, Oak Ridge, TN 37831, U. S. A.*
[5] *Department of Physics and Astronomy, University of Kentucky, Lexington, KY*
[6] *National Synchrotron Light Source II (NSLS-II), Brookhaven National Laboratory, Upton, NY 11973*
[7] *Department of Physics, University of Colorado at Boulder, Boulder, CO 80309*

(Dated: January 25, 2017)

Here we present further information on the sample characterizations and the first-principles calculations.

I. SAMPLE CHARACTERIZATION

The synthesis methods for the $Sr_2Ir_{1-x}Ru_xO_4$ single crystals were described in detail in Ref. 1. In Fig. S1, we adopt the enlarged unit cell that takes into account the $\sqrt{2} \times \sqrt{2} \times 2$ reconstruction in Sr_2IrO_4. The data was collected off resonance with an incident photon energy of 10 keV. Sr_2IrO_4 and $Sr_2Ir_{0.5}Ru_{0.5}O_4$ have comparable mosaics (as shown in the full widths of peaks in Fig. S1) for both structural Bragg peaks (0 0 12) and (1 1 18). Two crystal domains were observed in the Sr_2IrO_4 sample shown in Fig. S1. This splitting is considerably smaller than the momentum resolution used for the RIXS, so it should not lead to significant changes in the spectra presented.

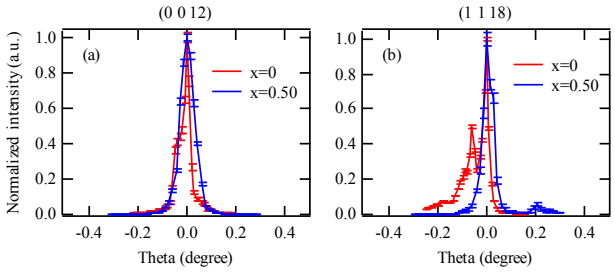

FIG. S1. X-ray diffraction rocking curves at (a) (0 0 12) and (b) (1 1 18). The peaks for the Sr_2IrO_4 and $Sr_2Ir_{0.5}Ru_{0.5}O_4$ are offset to zero, and the intensities are normalized to the corresponding peak intensities.

II. MAGNETIC EXCITATIONS IN Sr_2IrO_4

We present RIXS spectra from Sr_2IrO_4 synthesized using similar methods in Fig. S2 at select $\boldsymbol{Q}$-points. The magnon dispersion and width is comparable with those from earlier reports [2,3]. The data was collected at the Ir L_3 edge at the 27-ID-B beamline of the Advanced Photon Source. The incident X-rays were monochromatized using a Si(844) channel cut, achieving a total energy resolution of ∼30 meV. We choose a higher resolution (vs. the 80 meV resolution used in $Sr_2Ir_{1-x}Ru_xO_4$) as the magnetic excitations in Sr_2IrO_4 are considerably sharper (and in theory, energy-resolution limited). For an accurate determination of the magnon energy relative to the elastic energy, we place the energy analyzer around 85° to deliberately increase the photon counts at the elastic line. The momentum resolution is 0.23Å^{-1} and the sample is kept at ∼13 K, similar to the setup used for the $Sr_2Ir_{1-x}Ru_xO_4$.

We fit the elastic line using a Gaussian, and the magnon using a Lorentzian. Lorentzian is the intrinsic line shape of a magnetic excitation[4]. In the case of $Sr_2Ir_{1-x}Ru_xO_4$, a Gaussian is used for the magnetic excitation, due to the appreciable broadening from local Ru disorders.

III. FIRST-PRINCIPLES CALCULATIONS WITH MINIMAL SUPERCELLS FOR $Sr_2Ir_{1-x}Ru_xO_4$

This section presents the details of the first-principles calculations. To model the presence of Ru disorders in $Sr_2Ir_{1-x}Ru_xO_4$, we construct minimal supercells from the unit cell of Sr_2IrO_4, replacing Ir by Ru at selected sites. While the modified supercells are far from fully addressing the role of disorder over a large length scale, this construction captures the local interplay between the

t_{2g} bands of Ir and Ru atoms.

The calculations are performed using the WIEN2k[5] implementation with generalized gradient approximation[6] (GGA) + U potential. We consider the Ir/Ru density of states assuming both paramagnetic (PM) and spin-polarized (SP) ground states. A $8\times8\times2$ mesh of k-points is used for the calculation with the Ru $x = 0.25$ supercell, and a $12 \times 12 \times 2$ k-mesh is used for the $x = 0.50$ supercell.

Fig. S3 shows a single layer of supercell for $x = 0.25$ and $x = 0.50$ in the non-magnetic calculations. Notice that in the $x = 0.50$ supercell, we place the Ir and Ru sites on a checkerboard lattice such that the nearest neighbors of a Ru/Ir site are all Ir/Ru sites. Like in the parent Sr_2IrO_4, four layers are stacked along the c-direction in the supercells. Our calculations with an isolated Ir-Ru-O layer and different configurations of stacked layers all show minimal differences in the valence and magnetic moments in the ground state, indicating the interaction between layers is weak and the stacking is not essential for our purpose.

We depict the Ir $5d$ and Ru $4d$ density of states (DOS) from the non-magnetic ground state in Fig. S4 and Fig. S5. The Ir $5d$ DOS is projected onto the $J_{\rm eff} = 1/2$ and $J_{\rm eff} = 3/2$ states:

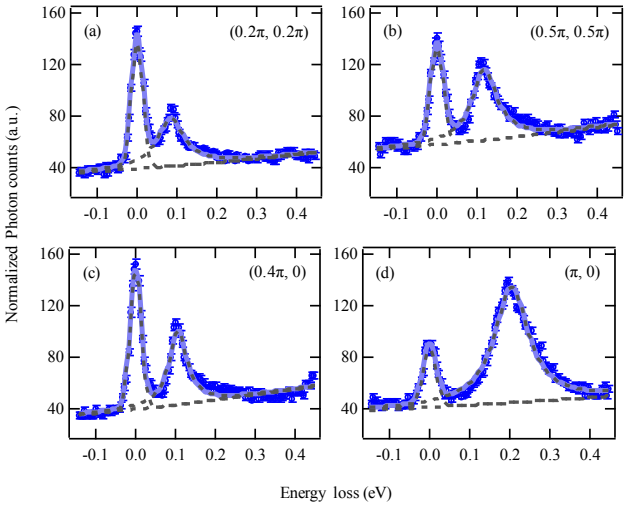

FIG. S2. (a)-(d) Energy loss spectrum of Sr_2IrO_4 at select $\boldsymbol{Q}$-points. The light blue solid lines are fits to the RIXS curves. The dashed grey lines mark individual components of the fit, as well as the smooth background.

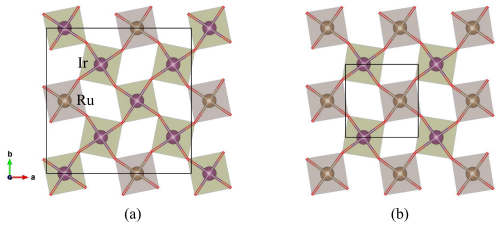

FIG. S3. Supercells for (a) $x = 0.25$ and (b) $x = 0.50$. The purple and brown circles represent the Ir and Ru atoms respectively. The solid black squares mark the supercells.

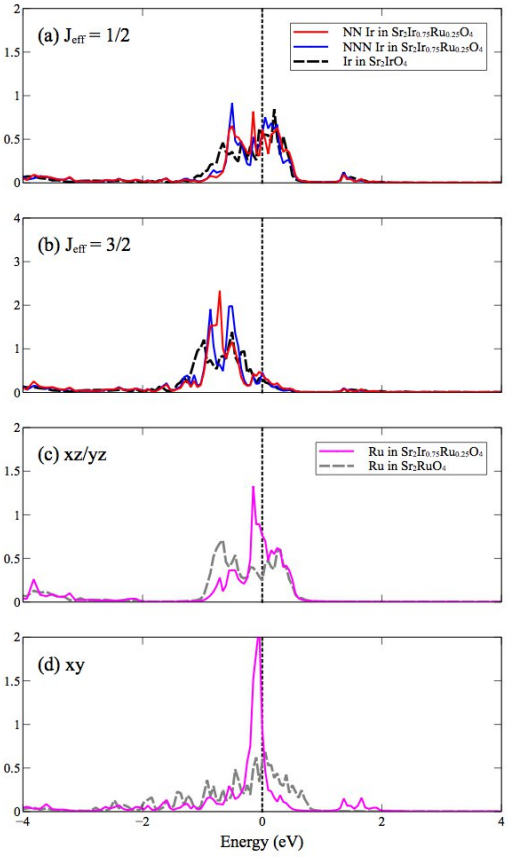

FIG. S4. Projected density of states in $x = 0.25$ supercell. "NN Ir" and "NNN Ir" denote Ir atoms that are nearest neighbors / next-nearest neighbors of Ru in the supercell.

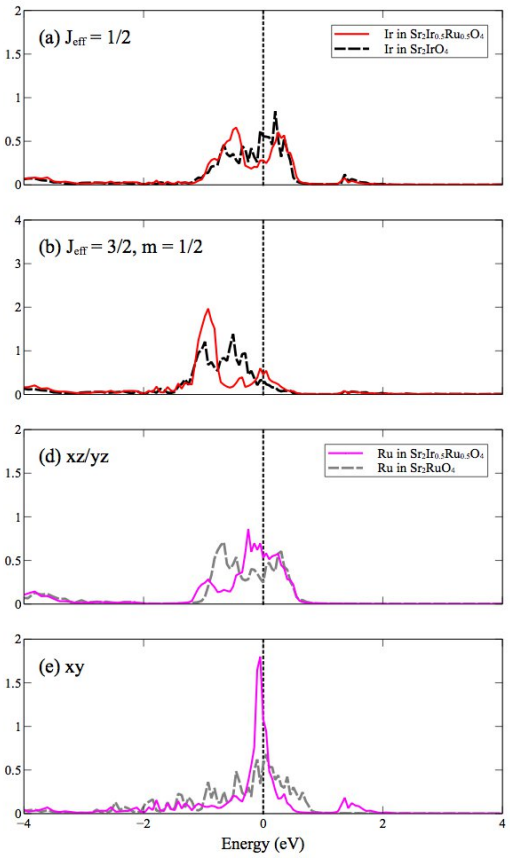

FIG. S5. Projected density of states for $x = 0.50$ supercell.

$$|J_{\rm eff} = 1/2, m = \pm 1/2\rangle = \sqrt{\frac{1}{3}}\left(\mp|xy, \pm\sigma\rangle - i|xz, \mp\sigma\rangle \pm |yz, \mp\rangle\right), \quad (1)$$

$$|J_{\rm eff} = 3/2, m = \pm 1/2\rangle = \sqrt{\frac{2}{3}}|xy, \pm\sigma\rangle + \sqrt{\frac{1}{6}}\left(\mp i|xz, \mp\sigma\rangle + |yz, \mp\sigma\rangle\right), \quad (2)$$

$$|J_{\rm eff} = 3/2, m = \pm 3/2\rangle = \sqrt{\frac{1}{2}}\left(\mp i|xz, \mp\sigma\rangle + |yz, \pm\rangle\right). \quad (3)$$

The Ru 4*d* DOS is projected onto the t_{2g} states. In the $x = 0.25$ supercell, there are two inequivalent groups of Ir atoms. One group is the nearest neighbors of the Ru sites, and the other is the next-nearest neighbors. As shown in Fig. S4 and Fig. S5, there are only slight changes in the projected Ir $J_{\rm eff}$ DOS in the $x = 0.25$ and $x = 0.50$ supercells, as compared to those in Sr_2IrO_4. The $J_{\rm eff} = 1/2$ state remains partially filled while the $J_{\rm eff} = 3/2$ states are almost filled for both groups of Ir atoms. The Ru t_{2g} states are more localized than those in the parent Sr_2RuO_4, suggesting the electrons are confined to the Ru sites. In the non-magnetic GGA+U calculation, even with a Coulomb interaction $U \gtrsim 3$ eV, there is no Mott gap for the $J_{\rm eff}$ orbitals. Besides, the non-magnetic DOS is not sensitive to the choice of U. Thus the dynamical effects of the Coulomb interaction are vital for a complete description of the Mott physics in Sr_2IrO_4, as discussed in Ref. 7. Here with the non-magnetic GGA+U calculation, we stress that the local electronic states on the Ir sites are barely affected by the proximate Ru sites, and that the low-energy physics stems from the partially filled $J_{\rm eff} = 1/2$ state.

We further perform calculations assuming spin-polarized (SP) ground states to investigate the formation of magnetic moments on the Ru sites. For the $x = 0.25$ supercell, we initialized the lattice with antiferromagnetic (AFM) order and a non-magnetic vacancy on the Ru site. After convergence, the Ru site develops a strong magnetic moment. The spin moment on Ru is $M_{spin,Ru} \simeq 1.45\mu_B$, and the spin moment on its nearest neighbor Ir is $M_{spin,Ir} \simeq 0.35\mu_B$. The spin moments on Ru and Ir are parallel, indicating an ferromagnetic coupling between the spin moments, and an antiferromagnetic coupling between the Ru spin and the Ir pseudospin. The same magnetic coupling is found in the $x = 0.50$ supercell.

IV. BREAKDOWN OF THE ANTIFERROMAGNETIC BRILLOUIN ZONE

In Sr_2IrO_4 and Ru-doped samples (below 0.50 Ru substitution) there is a $\sqrt{2} \times \sqrt{2} \times 2$ reconstruction due to the rotation of the Ir-O octahedra. As such, under the tetragonal convention, the structural and antiferromagnetic Brillouin zones overlap, and the electronic structures and magnetic excitations at the two Q vectors $(0, 0)$ and (π, π) should be equivalent.

In terms of the magnetic excitation, while the RIXS intensity $S(\mathbf{Q}, \omega)$ is different at these two Q-points, the energy of the excitation should be identical, as observed in the parent Sr_2IrO_4[2,3]. Thus it is quite unusual that the magnetic excitation energies at $(0, 0)$ and (π, π) are not identical in the $x = 0.27$ sample. This signals a breakdown of the antiferromagnetic Brillouin zone, which is well-defined *only* under translation symmetry. Admittedly, this effect is not captured in the current CPA calculation. However, in the carrier-doped Mott insulators (without octahedral rotations), where the antiferromagnetic Brillouin zone is also ill-defined, there are theoretical proposals showing different magnetic excitation energies at $(0, 0)$ and (π, π). For example, using more rigorous determinant quantum Monte Carlo methods, Jia *et al.*[8] interpreted the meltdown of the antiferromagnetic Brillouin zone as associated to the change in spin correlation from antiferromagnetic to ferromagnetic. Such an effect can also be shown in the Schwinger boson treatment of the square-lattice quantum antiferromagnet using the ferromagnetic configuration instead of the Néel state as the reference state, in which the long-range antiferromagnetic order is generated via Bose-Einstein condensation

at (π, π) with a considerable spin gap at $(0, 0)$[9].

For the single-electron spectral function $A(\mathbf{k}, \omega)$, as measured using angle-resolved photoemission spectroscopy, the intensity in the first and second structural Brillouin zone should be entirely identical as a matter of principle, apart from the matrix element prefactor. In Ref. 10, it was observed that the tetragonal structural Brillouin zone also fails to describe the complete electronic structures in these (effectively) carrier doped Sr_2IrO_4. Pseudogaps open at different locations in the first and second structural Brillouin zones, making the single-electron spectral function no longer equivalent in these two zones. Similar spectral function arrangement can be observed in the data set presented in Ref. 11 and 12, though not stated in the papers.

These observations go beyond conventional theory, but is something quite profound, and less mentioned.

* ycao@bnl.gov
† xliu@aphy.iphy.ac.cn
‡ wenhuxu@bnl.govn
§ mdean@bnl.gov

[1] S. J. Yuan, S. Aswartham, J. Terzic, H. Zheng, H. D. Zhao, P. Schlottmann, and G. Cao, Phys. Rev. B **92**, 245103 (2015).
[2] J. Kim, D. Casa, M. H. Upton, T. Gog, Y.-J. Kim, J. F. Mitchell, M. Van Veenendaal, M. Daghofer, J. van den Brink, G. Khaliullin, *et al.*, Phys. Rev. Lett. **108**, 177003 (2012).
[3] J. Kim, M. Daghofer, A. H. Said, T. Gog, J. van den Brink, G. Khaliullin, and B. J. Kim, Nat. Commun. **5**, 4453 (2014).
[4] L. J. P. Ament, M. van Veenendaal, T. P. Devereaux, J. P. Hill, and J. van den Brink, Rev. Mod. Phys. **83**, 705 (2011).
[5] P. Blaha, K. Schwarz, G. Madsen, D. Kvasnicka, and J. Luitz, An augmented plane wave+ local orbitals program for calculating crystal properties (2001).
[6] J. P. Perdew, K. Burke, and M. Ernzerhof, Phys. Rev. Lett. **77**, 3865 (1996).
[7] H. Zhang, K. Haule, and D. Vanderbilt, Phys. Rev. Lett. **111**, 246402 (2013).
[8] C. J. Jia, E. A. Nowadnick, K. Wohlfeld, Y. F. Kung, C.-C. Chen, S. Johnston, T. Tohyama, B. Moritz, and T. P. Devereaux, Nat. Commun. **5**, 3314 (2014).
[9] W.-G. Yin, H. Biao, and C.-D. Gong, Phys. Lett. A **220**, 281 (1996).
[10] Y. Cao, Q. Wang, J. A. Waugh, T. J. Reber, H. Li, X. Zhou, S. Parham, S.-R. Park, N. C. Plumb, E. Rotenberg, A. Bostwick, *et al.*, Nat. Commun. **7**, 11367 (2016).
[11] A. de la Torre, S. McKeown Walker, F. Y. Bruno, S. Riccó, Z. Wang, I. Gutierrez Lezama, G. Scheerer, G. Giriat, D. Jaccard, C. Berthod, *et al.*, Phys. Rev. Lett. **115**, 176402 (2015).
[12] Y. K. Kim, N. H. Sung, J. D. Denlinger, and B. J. Kim, Nat. Phys. **12**, 37 (2016).